

explore completely different ways of studying winds and astrospheres. The Atacama Large Millimeter/submillimeter Array (ALMA) may provide detections of free-free emission from winds, or at least provide much lower upper limits for stellar mass-loss rates. An even more sensitive radio telescope will ultimately be required to directly detect emission from winds as weak as that of the Sun.

Effects of stellar eruptions throughout astrospheres

OFER COHEN

Stars like the Sun evolve from young, fast-rotating and very active stars to older, slowly rotating main-sequence stars like our own Sun. The changes in stellar magnetic fields and stellar activity of such solar analogs with stellar evolution and the change in their rotation period are described in Ch. 2 of Vol. III. In this chapter, we review how the changes in stellar activity of Sun-like stars over stellar evolution translate to changes in their stellar winds, the structure of their interplanetary space and of their astrospheres, the transport of particles, and the propagation and evolution of coronal mass ejections (CMEs). We also review the consequences of CMEs in stellar systems other than our own and their role in planet habitability.

Since the dawn of the space exploration era, great knowledge has been acquired about the solar system's interplanetary space and the heliosphere. The growing amount of spacecraft in-situ measurements of the interplanetary medium (direct measurements of solar-wind particles; see reviews by McComas *et al.*, 2007, and Owens and Forsyth, 2013), as well as increasing amount of global remote-sensing observations monitoring the Sun's photospheric magnetic field, EUV and X-ray coronal radiation, radio emissions, and energetic particles (reviewed by, e.g., Lang, 2009) have revealed a clear dependence of the state of the heliosphere and the interplanetary space on the solar activity level and on the solar magnetic-field structure. These long-term observations also revealed how the frequency of solar eruptions change over the solar cycle (see the review by Webb and Howard, 2012).

4.1 Astrospheres in time

4.1.1 *Astrospheric structure and evolution with time*

The extent and structure of astrospheres are determined by the radially expanding super-Alfvénic stellar wind that drags the stellar magnetic field from the stellar corona through the interplanetary medium, until the wind is stopped by the

interstellar medium (ISM; see Ch. 3). It is also determined by the rotation of the star. As a result, each astrospheric magnetic field (AMF) line has one end (or “footpoint”) attached to the stellar surface, while its location at each point in the astrosphere, $\mathbf{r}(r, \theta, \phi)$ (for co-latitude θ), is given by the following formula. It describes a spiral shape and is known as the “Parker Spiral” (Parker, 1958):

$$\mathbf{B}(r) = B_0 \left(\frac{r_0}{r} \right)^2 \left[\hat{r} + \frac{(r - r_0)\Omega \sin \theta}{v} \hat{\phi} \right]. \quad (4.1)$$

Here Ω is the stellar rotation rate (angular velocity), v is stellar-wind speed (which is here assumed to be radial and fixed in time); r_0 is the actual base point of the AMF, and is at a reference distance from the stellar surface at which we assume the stellar wind is fully developed and has achieved its asymptotic speed and radial direction; B_0 is the magnetic field magnitude at that point. We can see that the radial component of the AMF has an r^{-2} dependence, while the azimuthal component has only a r^{-1} dependence. As a result, through most of the astrospheres, the AMF is dominated by the azimuthal field, which is a function of Ω , except for high latitudes (small θ) where the AMF lines are nearly radial.

Over time, stellar-rotation periods vary from less than one day for very active, young stars to about 20–100 days for older, main-sequence stars like the Sun. For very fast rotating stars, the AMF spiral is completely dominated by the azimuthal component: the field is highly compressed, and its azimuthal component dominates even at relatively small distances from the star and inside the stellar corona, which typically extends to 10–20 stellar radii (Cohen *et al.*, 2010a). In this case, even extended closed magnetic loops can be bent as a result of the fast rotation. This effect can have implications for the triggering of very strong stellar flares, and for the mass-loss rate of the star to the stellar wind (see e.g., Maggio *et al.*, 2000; Matranga *et al.*, 2005; Cohen *et al.*, 2010a,b). The left-hand panel in Fig. 4.1 shows how the compression of the AMF spiral changes for different stellar rotation periods. The other two panels show the AMF lines close to the star (up to 24 stellar radii). It can be clearly seen that the field lines are nearly radial for the slow, solar-like rotation period of 25 days, while the field lines are strongly bent in the azimuthal direction for fast rotation period of half a day.

Equation (4.1) describes how a given magnetic field line changes with distance for a given value of B_0 at its base (r_0), and a given asymptotic stellar wind speed v . However, the AMF is formed by a collection of field lines that are defined by some spherical distribution of B_0 at the base of the stellar corona. This distribution depends on the topology of the stellar magnetic field at a given time. In addition, the value of v also varies as it empirically depends on the expansion of the magnetic flux tubes and on the non-uniform distribution of B_0 (Wang and Sheeley, 1990). For the Sun, the distribution of B_0 changes dramatically over the solar cycle. This

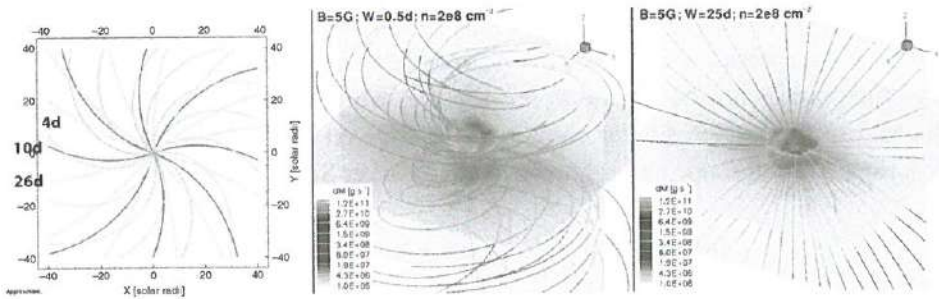


Fig. 4.1 Left: conceptual display of different stellar-wind magnetic field spirals for a Sun with a 4.6-day rotation period, a 10-day period, and a 26-day period, as a function of distance in solar radii (from Cohen *et al.*, 2012). Center/right: results from numerical simulations for the stellar coronae of solar analogs with rotation period of 0.5 day (A) and 25 days (B). The astrospheric field lines are shown in gray. Also shown is the surface at which the Alfvénic Mach number equals unity. In the original figure (Cohen and Drake, 2014) the meridional and equatorial planes are colored with contours of the mass-loss rate, but these are not adequately reproduced in this gray-scale rendering.

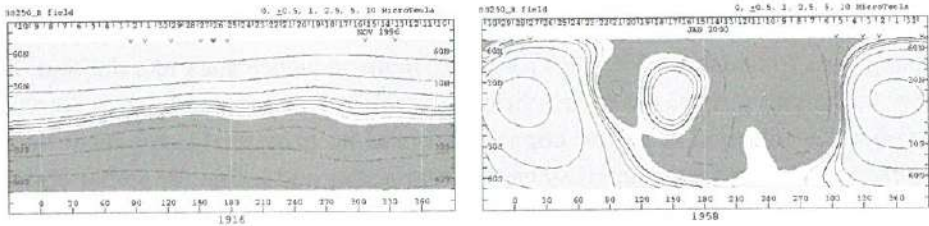


Fig. 4.2 The distribution of the solar magnetic field at $r = 2.5R_{\odot}$ (B_0) for solar minimum period (left, November 1996), and solar maximum period (right, January 2000) obtained by the Wilcox Solar Observatory (WSO, wso.stanford.edu).

can be seen in Fig. 4.2, which shows the distribution of the solar magnetic field at a distance of $r_0 = 2.5R_{\odot}$ for solar minimum period (November 1996) and for solar maximum period (January 2000).

Over time, stellar activity appears at different latitudes, while changing in magnitude as the behavior of surface magnetic activity is highly tied to the rotation rate. Young active stars seem to have very strong large-scale magnetic fields with magnitude of several kilo-gauss. For reference, the Sun's dipole field strength is of the order of 5–10 G, and while the magnetic flux density within active regions can be high (ranging up to well over a kilo-gauss in sunspots), solar active regions are rather small in size. In addition, magnetic activity in active stars tends to appear at high-latitude, polar regions (Strassmeier, 1996, 2001, Donati and Collier Cameron, 1997). This behavior is most likely related to the role of the fast stellar rotation

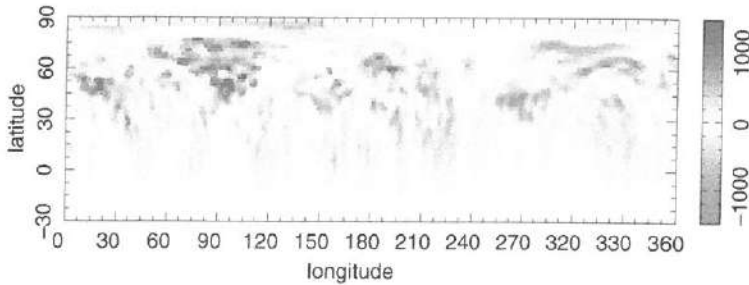


Fig. 4.3 Longitude–latitude map of the photospheric radial magnetic field of AB Doradus. Note that field in the deep southern hemisphere cannot be observed owing to the tilt of the spin axis. (From Hussain *et al.*, 2007.)

in the stellar dynamo and meridional magnetic flux circulation (Schuessler and Solanki, 1992; Solanki *et al.*, 1997; Schrijver and Title, 2001), see also Ch. 2.6, Vol. III. An example of such a young active stars is AB Doradus, which is a 50-Myr-old K0 dwarf star rotating with a half a day period. Figure 4.3 shows the photospheric distribution of the radial stellar magnetic field taken from Hussain *et al.* (2007). One can see that there is a great coverage of magnetic field of over a kilo-gauss in magnitude, and that these strong field regions appear at latitudes higher than 45 degrees and up to 75–80 degrees from the equator, in contrast to solar active regions, which do not appear above 30 degrees from the equator (cf., Fig. 2 in Vol. III). See also Fig. 4.4.

The appearance of stellar activity described above reflects a change in the distribution of B_0 . Therefore, it affects the shape of the AMF and the astrosphere volume. It is not clear how v changes for young stars as we cannot directly measure stellar winds of “cool stars”, i.e. stars with a convective envelope beneath their surfaces such as in the case of the Sun. Some techniques to estimate mass-loss rates from cool stars are described in Ch. 3. However, these estimates do not separate the stellar-wind speed from the density, so it cannot be obtained independently. Another cause for the lack of estimates for stellar wind speeds of cool stars is the incomplete theory about the solar wind acceleration (see Vol. I, Ch. 9). In order to demonstrate how the change in the photospheric field affects the three-dimensional structure, Fig. 4.5 shows the distribution of the photospheric magnetic field and the shape of the three-dimensional magnetic field close to the Sun. The left panel is obtained using actual data of the photospheric field during high solar activity period. In the other two panels, the original data were manipulated, so that the active regions have been shifted by 30 and 60 degrees, respectively, towards higher latitudes in order to mimic the activity distribution of young active stars. It can be seen that the field topology changes dramatically even if only the positions of the active regions are changed.

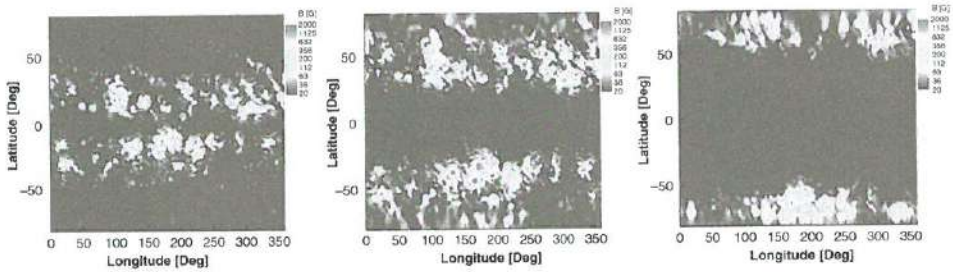


Fig. 4.4 A map of the solar photospheric radial magnetic field (magnetogram) during Carrington Rotation 1958 (January 2000, solar maximum period) shown on the left. The middle and right panels show manipulation of the original map, where the active regions have been shifted by 30 and 60 degrees towards the pole, respectively. (From Cohen *et al.*, 2012.)

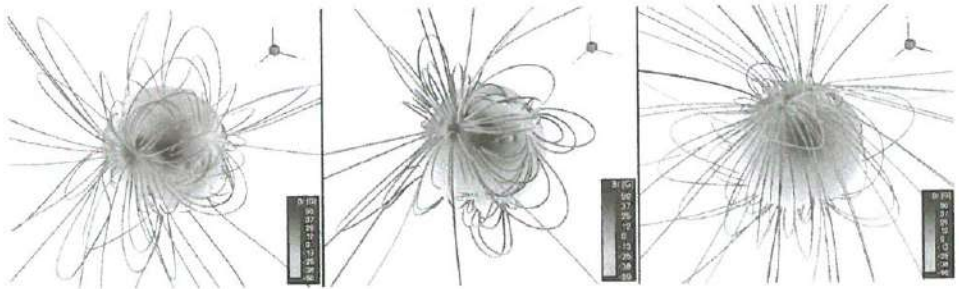


Fig. 4.5 The three-dimensional magnetic field corresponding to the surface distribution of the photospheric radial magnetic field (shown on a sphere of $r = R_{\odot}$) during solar maximum (left), and for manipulated photospheric field with the active regions shifted by 30 degrees (middle) and 60 degrees (right) towards the poles, as shown in Fig. 4.4. (From Cohen *et al.*, 2012.)

4.1.2 Astrospheric evolution and particle transport

Ch. 9, Vol. II and Ch. 9, Vol. III describe transport processes of energetic particles in the solar system and in particular, Galactic Cosmic Rays (GCRs), which carry energies of up to 10^{21} eV. It has been known for many years that the lower part of the GCR energy spectrum (about 1 GeV), is modulated by the state of the AMF and the solar wind. This happens because GCR transport depends on the state of the AMF via two terms in the transport equation described in Ch. 9, Vol. II. The drift term, which depends on the magnetic field magnitude and direction, dictates whether particles travel inwards or outwards near the heliospheric ecliptic plane, and whether GCRs approach the ecliptic plane (and the vicinity of the Earth) from equatorial regions or from polar regions, depending on the polarity and magnitude of the AMF. The diffusion term (and the diffusion coefficient) depend on the

field magnitude, and has components parallel and perpendicular to the mean local magnetic field. The drift and diffusion terms are responsible for the clear GCR modulation over the solar cycle, where the GCR intensity anti-correlates with the sunspot number (see Fig. 9.4 in Vol. III). The reduction in GCR intensity during high solar activity (solar maximum) is a result of the increase in the AMF magnitude as the Sun sheds more magnetic flux into the heliosphere, the increase in the number of interplanetary shocks (i.e., increase in CME rate), and the overall increase in the level of turbulence in the solar wind. All of the above make it harder for GCRs to penetrate deep into the heliosphere all the way to the Earth. During solar minimum, the AMF reduces to its floor value, and the CME rate decreases as well. This improves the ability of GCRs to penetrate into the heliosphere so their intensity increases during low solar activity periods. Voyager 1 has provided us with a direct observation of how the GCR intensity changes with distance from the Sun inside the heliosphere. Figure 4.6 shows the dramatic increase in GCR intensity accompanied by a similar sharp drop in the intensity of solar wind particles. This is one of the indications that Voyager 1 has indeed, left the solar system and is currently in the ISM.

The Earth is shielded from most energetic GCRs by its own magnetic field, and by the AMF. Nevertheless, some cosmic rays with very high energies can reach the top of the Earth's atmosphere and generate a cascade reaction with atmospheric particles (air shower, see Ch. 11 in Vol. III). There are a number of ways that GCRs have played a role in the evolution of Earth. They can be an ionization source for the production and creation of complex organic molecules and nucleotides (e.g., Court *et al.*, 2006; Simakov *et al.*, 2002), can cause cellular mutation through direct and indirect processes (e.g., Nelson, 2002; Dartnell, 2011), and they can play a role in triggering lightning (e.g., Gurevich *et al.*, 1999; Dwyer *et al.*, 2012). It has been suggested that GCRs can contribute to global climate change periods in the Earth's history as they may change the Earth's albedo by affecting cloud condensation (Svensmark and Friis-Christensen, 1997; Shaviv, 2003, 2005b; Wallmann, 2004; Medvedev and Melott, 2007; Kirkby *et al.*, 2011). This subject is still under debate, where the argument focuses on the magnitude of this effect and whether it is significant or not.

In the previous section, we have shown how the AMF changes with time as a result of the increase in stellar rotation and stellar magnetic topology. Let us focus on a particular period of time in Earth's history called the Archean eon, which spanned from about 3.8 to 2.5 billion years ago. This period of time occurred right after the Late Heavy Bombardment (the time when the Earth was continuously hit by solar system small bodies), and when it is believed that simple life forms began to emerge (see Ch. 4, Vol. III). With the above effects of GCRs on the Earth atmosphere, it is useful to estimate the GCR intensity near Earth during the Archean eon.

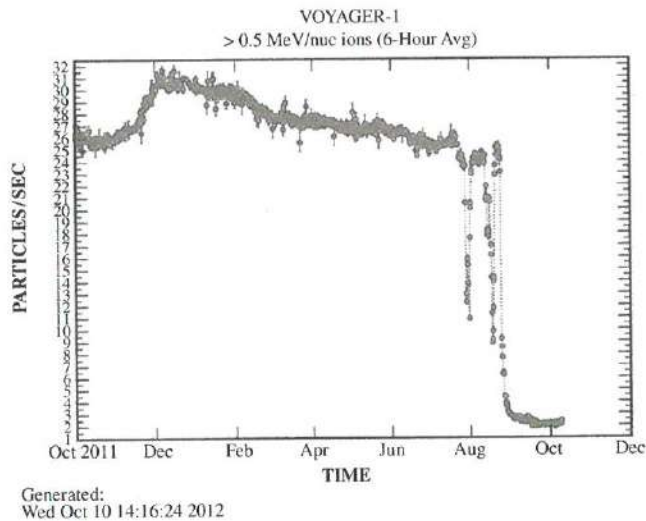
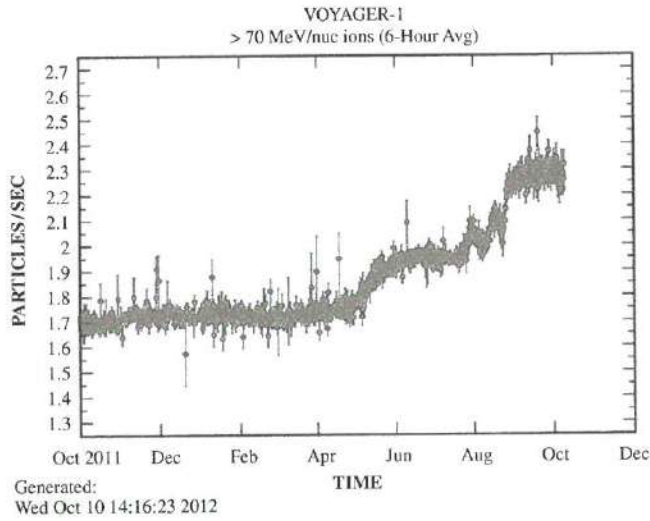


Fig. 4.6 The dramatic increase in cosmic-ray flux (top) and decrease in solar-wind particle flux (bottom) observed by Voyager 1 around September 2012. This observation strongly suggests that *Voyager 1* reached the ISM at the time of the change. (Figures from science.nasa.gov.)

During that time, the solar rotation was 2–4 times faster, with rotation period of about 6–15 days in contrast to the current 25 day period. In addition, based on astronomical observations of solar analogs of that age, the magnetic activity seems to appear at higher latitudes. Based on this information, Cohen *et al.* (2012) used the solar magnetohydrodynamic (MHD) model and GCR transport model to calculate the GCR intensity near the Archean Earth as a function of a solar rotation period, and the topology of the Sun’s magnetic field. They used solar magnetic

field data and split them into a weak, dipole component, and a strong, “spots” component which represents active regions. They then shifted the spots component in latitude (as seen in Fig. 4.4), and also modified the magnitude of each component to study the effect of the spot location and magnitude of the weak and strong solar field on the GCR transport and intensity.

Figures 4.7 and 4.8 show the results for the GCR intensity near the Archean Earth. They show that the dominant effect is the change in solar rotation rate, which dramatically reduces the intensity peak around 1 GeV by two orders of magnitude. The results also show that in the case of fast rotation (2 days), the Earth is completely shielded from GCRs with energies of less than about 20 MeV. The intensity reduction is enhanced even further if the magnitude of the solar active regions is increased, where almost all the GCRs are prevented to reach Earth, except for those with energies above 1 GeV or so.

The results shown here quantify and clearly demonstrate how the increase in solar rotation and solar magnetic activity lead to a significant reduction of GCR penetration to the inner heliosphere during the early solar system. Therefore, the role of GCRs in the evolution of the Earth’s atmosphere and the evolution of life on Earth (via the processes mentioned above) has increased with time.

4.1.3 *Stellar activity and disk evolution*

In Section 4.1.2, we discussed how fast rotation and strong magnetic fields, in particular in the polar regions, of young stars significantly increase their AMF. Pre-main-sequence stars hosting accreting disks (also known as Classical T-Tauri Stars – CTTS; cf., Ch. 3 in Vol. III) have relatively fast rotation, with rotation periods ranging from 7 to 10 days, strong surface flux intensity observed to be more than 0.5 kG and, in many cases, frequent large flaring that may be due to the interaction between the disk and the stellar magnetosphere (see the review by Hussain, 2012).

In protoplanetary disks of such young stars, angular momentum transport controls the transfer of material to and from different regions of the disk (Bodenheimer, 1995). Therefore, it is crucial to understand the evolution of disk angular momentum transfer in order to understand the evolution and formation of planetary systems and the origin of planets. Some of the more popular mechanisms to explain disk angular momentum transfer involve an interaction between magnetic fields in the disk and the disk’s gas. Among them are turbulence as a result of the so-called magneto-rotational instability (MRI, Balbus and Hawley, 1991), large-scale magnetic field driving outflow that causes stress (Blandford and Payne, 1982), or disk shearing (Turner and Sano, 2008) (see also Ch. 3, Vol. III). However, these processes require strong coupling between the disk’s gas and the magnetic field, and

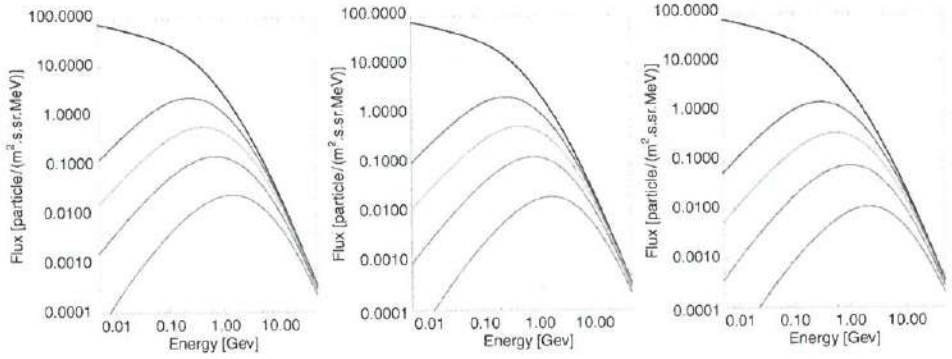


Fig. 4.7 Cosmic-ray energy spectrum for modeled solar rotation periods of 26 days (current rotation), 10 days, 4.6 days, and 2 days, along with the local ISM spectrum. Plots are for the current Sun (left), spots shifted towards the pole by 30 degrees (middle), and spots shifted towards the pole by 60 degrees (right). This plot is similar to Fig. 11.11 in Vol. III, except that the x -axis unit is in GeV instead of MeV, and the flux is normalized by the additional steradian (sr) geometrical factor.

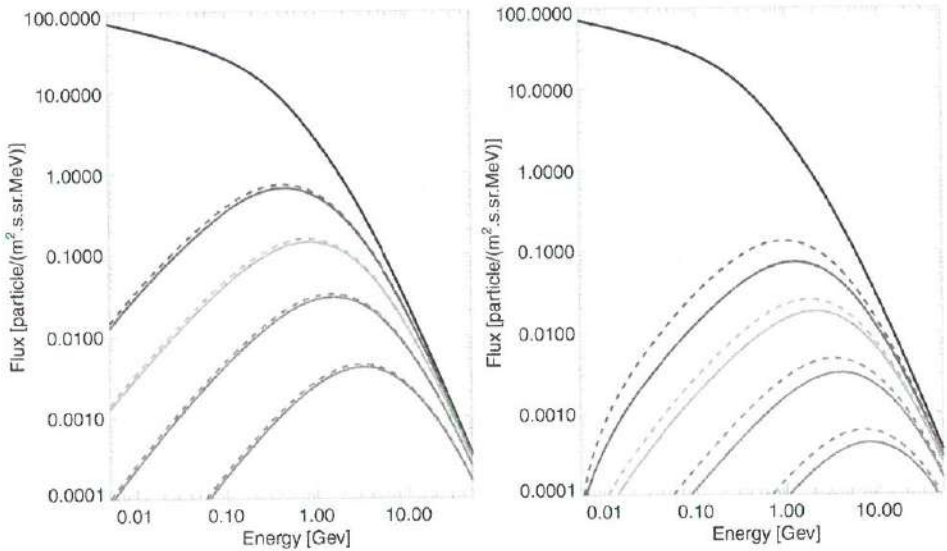


Fig. 4.8 Same as the right-hand panel of Fig. 4.7, but with the dipole component enhanced by a factor of 10 (left), and the spot component enhanced by a factor of 10 (right). Solid lines represent the spectrum with the Termination Shock (TS) scaled with the solar-wind dynamic pressure, while dashed lines represent the spectrum for the TS fixed at 90 AU.

such a coupling requires the gas in the disk to be sufficiently ionized: if the disk's gas is neutral it cannot interact with the electromagnetic force.

One potential source of disk ionization is GCRs, which penetrate from the edge of the stellar system to the vicinity of the disk near the equator. Other possible

sources for disk ionization are heat, X-ray radiation originating from the corona of the central star, and the decay of radionuclides within the gas (Turner and Drake, 2009; Cleeves *et al.*, 2013). GCRs and X-ray radiation are expected to penetrate up to certain depth from the top of the disk, creating a disk “skin”, which is sufficiently ionized to couple the magnetic field and the gas, and an inner “dead zone”, where the gas is neutral and the magnetic field is essentially irrelevant (see e.g., Gammie, 1996; Sano *et al.*, 2000; Ilgner and Nelson, 2006; also compare Fig. 5.9). Because the magnetic fields of CTTS are strong, and their rotation periods are rather short, the intensity of GCRs may not be sufficient to ionize the disk. Owing to this, the impact of the stellar wind and the AMF on disk ionization by GCRs is usually neglected, where ISM GCR intensities are used to estimate ionization rates.

Turner and Drake (2009) have tested all of the above disk-ionization mechanisms, as well as ionization by energetic protons originating from the corona of the central star. They found that a dead zone is created in all scenarios, as well as an undead zone at which resistivity is high enough to allow shear-generated large-scale magnetic field, but it hampers MRI turbulence. However, they found that while the necessary conditions to couple the magnetic field and the gas are feasible, they are in some conflict with the conditions necessary for planet formation in the disk as the solution without a dead zone requires surface density below the minimum mass defined by a protosolar model (Fromang *et al.*, 2002). In other words, the density necessary for sufficient gas ionization should be low, but the density necessary for planet formation in the disk should be high. Cleeves *et al.* (2013) calculated the GCR intensity and disk-ionization rates while taking into account the GCR flux reduction and modulation by the stellar wind and AMF. They found that the ionization rate by GCR is one order of magnitude less than the standard value used for disk ionization and chemistry. Therefore, it is not clear whether the extensive study of disks using the MHD formalism is valid everywhere in the disk.

In summary, while some sources of disk ionization, such as heat close to the central star, X-ray radiation, and energetic protons originating from shocks in the stellar corona, can ionize the inner part of the disk and are enhanced in CTTS, global ionization is more likely to occur due to GCRs. However, the high magnetic activity level of CTTS actually reduces the amount of ionizing GCRs that reach the disk in its inner parts and up to about 100 AU (the GCR intensities can be higher at the outer edge of the disk).

4.2 Coronal mass ejections in time

In general, stellar activity is quantified by the stellar total X-ray luminosity, L_x , which is an indication for the amount, strength, and temperature of hot coronal loops, and by the X-ray/EUV flaring rate and magnitude, which provide an

insight for coronal dynamic activity and its time scales. These “activity indicators” are known to be correlated with the stellar rotation rate and age (see Ch. 2, and Ch. 2, Vol. III). CMEs and large X-ray flares on the Sun are known to be correlated to each other (see Ch. 6, Vol. II). The traditional view on the generation of solar flares is that particles are accelerated down from the top of the CME flux-rope (as it propagates out) and hit the chromosphere, leading to “evaporation” of heated plasma, generating strong X-ray emissions. Because we cannot observe CMEs on other stars, stellar flares serve as proxies for CME activity on other stars.

In this section, we review the possible role of CMEs in stellar evolution, based on the known flaring activity (see Ch. 2 of this volume). We also review how the change in the interplanetary medium may affect the propagation and evolution of CMEs. As very little work has been done on studying stellar CMEs, this section is in part necessarily qualitative.

4.2.1 Initiation, propagation, and evolution of CMEs through different astrospheres

We can divide our overview on CMEs over time into two different categories. First, we can estimate how the change in stellar activity over time may impact the initiation, rate, and angular distribution of CMEs. Second, we can estimate how the change in the interplanetary medium over time affects the propagation and evolution of CMEs.

Let us first discuss how CMEs may be initiated differently in young, active stars. On the Sun, active regions appear within latitudes of about ± 30 degrees or less from the equator. These active regions are the source location of many CMEs and indeed, most CMEs appear to originate from within these latitudes (Gopalswamy *et al.*, 2008). As mentioned in Section 4.1.1, in young active stars, the magnetic activity appears at much higher latitude. Therefore, if we assume a similar relation between the location of the active regions and the source point of the CMEs, it is possible that most of the CMEs in such stars are launched from, and propagate into, the polar regions of the astrosphere (Fig. 4.9 shows a conceptual schematic of this difference). In any case, it is not possible to determine the latitudinal distribution of stellar flares due to the fact that observations represent the source integrated photon flux of what is essentially a point source.

Another aspect that is important to discuss is whether stellar flares, in particular large ones, are triggered by traditional, solar-like CMEs. The general CME initiation mechanism, while not completely understood, can be associated with a slow storage of magnetic energy via twisting of the CME flux-rope (by some kind of motions at the base of the magnetic loops), followed by a sudden release of

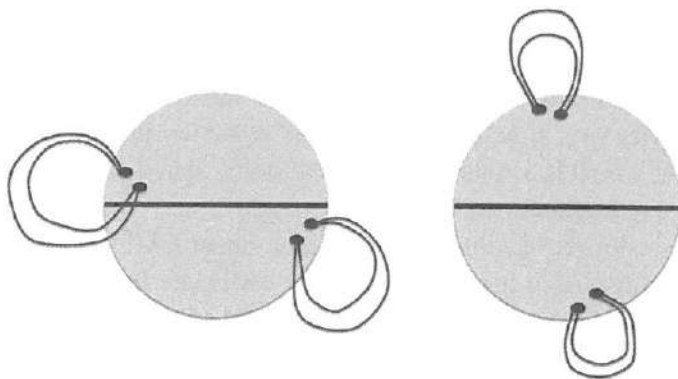


Fig. 4.9 On the Sun, CMEs are launched from active regions that emerge at low latitudes near the equator (left). In active young stars, magnetic activity appears at high, polar latitudes. Therefore, CMEs may be launched mostly towards the polar astrospheric regions (right).

the energy, most likely due to magnetic reconnection (see Ch. 6, Vol. II). We can imagine other, similar scenarios to trigger flaring activity. For example, the coronal loops of fast rotating stars are highly tangled in the azimuthal direction (as shown in Fig. 4.1). Such a tangling could build magnetic energy in the loops due to the increased magnetic tension. Similar to the way it triggers CMEs, magnetic reconnection could trigger a sudden release of the magnetic tension, triggering a very large flare as a result of the large size of the loop (these stretched loops can be of the order of the star size due to the strong stellar magnetic field). Cohen *et al.* (2010b) used an MHD model to simulate the corona of FK Comae, a rapidly rotating (2.4 days) late-type giant G star. These simulations showed that the azimuthal tangling of the large coronal loops indeed builds up high magnetic tension. While the steady-state simulation could not provide any dynamic triggering for reconnection, it is more than possible that such a triggering could occur due to footpoint motions on the photosphere. In CTTS, magnetic energy could slowly build up due to twisting or stretching of the field by the interaction between the stellar magnetosphere and the accretion disk (Hussain, 2012). As mentioned in Section 4.1.3, for such an interaction to occur, the disk gas should be sufficiently ionized. However, the interaction between the magnetosphere and the disk in the context of the flaring activity occurs at the inner part of the disk, where ionization levels are most likely sufficient.

Now we discuss how the state of the astrosphere itself affects CMEs. We keep in mind that CMEs carry with them new magnetic flux that is injected into the pre-eruption Astrospheric Magnetic Field (AMF). Therefore, we need to consider how changes in the state of the ambient AMF over time may impact the propagation and

evolution of CMEs. The AMF changes as a result of the change in stellar rotation rate, where the AMF spiral is more compressed for faster rotating, young stars and it is less compressed for older stars. The AMF also changes with the reduction in stellar activity over time (indicated by the reduction in flare rate and total X-ray/EUV flux, which is a consequence of the stellar spin down). In both cases, the end result is a reduction in the strength of the AMF.

To date, we do not have much information about CMEs on other stars (with the exceptions discussed in the next section). CMEs are the result of a buildup of non-potential energy that is released as the system relaxes to a lower energy state. The erupted magnetic flux is then carried by the CMEs and is added to the AMF flux via interchange reconnection (see Section 8.8, Vol. III). Therefore, with the addition of CME magnetic flux, the AMF strength is higher during solar maximum than its “floor” value during solar minimum when very little CME magnetic flux is added (Owens and Forsyth, 2013). It has been suggested that the reason for the record-low AMF strength during the extended solar minima between solar cycle 23 (1996–2007) and 24, i.e., from 2008 to about 2012, is due to the record-low number of CMEs during that period of time (Owens *et al.*, 2008).

We assume that CMEs, due to their role in regulating the system’s energy, scale with the overall available magnetic energy. In other words, if the overall stellar field is much stronger for young active stars, then we expect the magnetic flux in CMEs in these stars to be high accordingly. In this case, the role of CMEs in the evolution of the AMF (as discussed in Section 8.8, Vol. III) is probably similar to the case of the Sun, unless the CME rate in active stars is much greater so that the AMF never falls to its floor level. Alternatively, it is also possible that CMEs in active stars carry magnetic flux of similar magnitude to that of solar CMEs. This is possible if the large-scale strong fields observed on active stars are actually composed of many small-scale active region that are smeared out by the lack of high resolution. In this case, the role of CMEs in the evolution of the AMF is weaker for young active stars, the AMF is dominated by the floor value of the stellar ambient field, and the role of CMEs increases over time.

Active young stars have their AMF spiral more compressed with the azimuthal component of the AMF being dominant even at relatively close distances from the stars. Therefore, it is more likely that the radially and fast propagating CME will shock a slower stream of ambient stellar wind moving within the azimuthally tangled magnetic field. This process is similar to shocks driven by interacting solar wind streams known as Co-rotating Interaction Regions (CIRs, see Section 8.5.2, Vol. III). Based on this scenario, many more shocks are expected in the astrospheres of young, active, and fast rotating stars, with consequences for particle transport as discussed in Section 4.1.2. However, as mentioned above, it is possible that CMEs on such stars are launched at very high latitudes, where the AMF is nearly radial.

In that case, the interaction between CMEs and the AMF should be similar to that of the Sun.

4.2.2 The role of CMEs in stellar mass loss and stellar spin down

Over their lifetime, cool stars lose angular momentum and spin down (from rotation periods of less than a day to 20–100 days). The conventional mechanism for stellar spin down is that stars lose angular momentum to the magnetized stellar wind in the concept called “magnetic breaking” (Weber and Davis, 1967). In this process, the mass flux carried by the accelerating stellar wind drains angular momentum as long as the wind speed is below the Alfvén speed, $v_A = B/\sqrt{4\pi\rho}$ (in cgs units of cm s^{-1}), where B is the local magnetic field strength, and ρ is the local mass density. Once the wind speed equals the Alfvén speed at a point called the “Alfvén point”, coronal magnetic field lines that are carried and stretched by the wind open up, and all the mass at this point is considered lost from the star. Another way to look at this process is to think of the magnetic field lines as rods that are attached to the spinning star at one end, where the other ends of the open field lines are radially stretched beyond the Alfvén point. As a result, each field line applies torque on the star and spins it down. This torque is proportional to the momentum of the wind at the Alfvén point, to the stellar rotation rate, and to the distance of the Alfvén point (the lever arm that applies the torque). The imaginary surface that represents all the Alfvén points is called the “Alfvén surface” and the integral of the mass flux through this surface is the mass-loss rate, \dot{M} , of the star to the stellar wind. For a spherically symmetric wind, and a dipole stellar magnetic field, we can calculate the total torque on the star and the total angular momentum loss rate, \dot{J} :

$$\dot{J} = \frac{2}{3}\Omega\dot{M}r_A^2, \quad (4.2)$$

where Ω is the stellar rotation rate, r_A is the average distance to the Alfvén surface, and we assume constant moment of inertia. From Eq. (4.2) we see that the mass-loss rate is necessary to estimate the spin-down rate of a star. However, stellar winds of cool, Sun-like stars are very weak and cannot be directly observed (see previous chapter of this volume), which makes it challenging to estimate \dot{J} as a necessary input for stellar evolution models. It is also important to determine the mass-loss rates of young active stars in the context of the *Faint Young Sun paradox* (see Section 2.3.1 in Vol. III). The paradox arises from the stellar evolution models prediction that the young Sun was about 30% less luminous than current day, so the Earth’s surface temperature should have been below the freezing temperature of water. Nevertheless, we find geological evidences for the existence of liquid water on the surface. There are a number of solutions to the paradox, such as the existence

of atmospheric greenhouse gases that can increase the surface temperature. In the context of stellar mass-loss rates, a solution for the paradox is possible if we can demonstrate that the young Sun was about 10% more massive in the past, and it had a high mass-loss rate that led to its current mass (Graedel *et al.*, 1991; Wood *et al.*, 2002).

Based on indirect measurements mentioned in the previous chapter, theoretical models (Cranmer and Saar, 2011), and numerical models (see, e.g., Matt *et al.*, 2012; Cohen and Drake, 2014) have shown that mass-loss rates in Sun-like stars seem to fall in the range between 10^{-15} – $10^{-11} M_{\odot} \text{ yr}^{-1}$ (the present-day solar mass-loss rate is $(2-3) \times 10^{-14} M_{\odot} \text{ yr}^{-1}$; Cohen, 2011). However, stars can also lose mass via CMEs. In the case of the Sun, each CME carries some 10^{13} – 10^{17} g into space (Yashiro and Gopalswamy, 2009), with an annual integrated mass loss via CMEs of several percents of the ambient mass loss (Vourlidis *et al.*, 2010). Therefore, CMEs on the Sun play very little role in the solar mass loss. This role could become significant if the CME rate were higher by a factor of 10 or more. In this case, CMEs could even dominate the stellar mass loss.

In the section above, we discussed the possibility that not every stellar flare is a result of a CME. Nevertheless, stellar flares are still our only indication for CMEs on other stars. Keeping this in mind, let us assume that stellar X-ray flare rate also represents CME rate. In this case, we can investigate the relation between solar CMEs and solar flares, and extrapolate this information to other stars. Both Aarnio *et al.* (2012) and Drake *et al.* (2013) performed quite similar calculations to estimate stellar mass-loss rates due to CMEs; here we follow the formalism by Drake *et al.* (2013).

Based on observations from the Large Angle and Spectrometric Coronagraph Experiment (LASCO) on board the Solar and Heliospheric Observatory (SOHO) mission, and 1–8 Å X-ray data obtained by the GOES satellite, Yashiro and Gopalswamy (2009) and Aarnio *et al.* (2011) obtained a power-law relation for CME mass, m_c , as a function of the CME flare energy, E , in the GOES X-ray bandpass:

$$m_c(E) = \mu E^{\beta}, \quad (4.3)$$

with $\mu \approx 0.002 - 0.02$ and $\beta \approx 0.6$. Yashiro and Gopalswamy (2009) also found a power-law for the CME kinetic energy, E_k , as a function of the flare energy:

$$E_k(E) = \eta E^{\gamma}, \quad (4.4)$$

with $\eta \approx 10 - 30$ and $\gamma \approx 1$. Figure 4.10 shows the scatter and fit for the above power laws from Drake *et al.* (2013). The dashed line in the bottom panel represents constant ratio of CME kinetic energy to GOES X-ray energy loss. There is a constant factor of about 200 between the X-ray energy fit (dashed line) and the

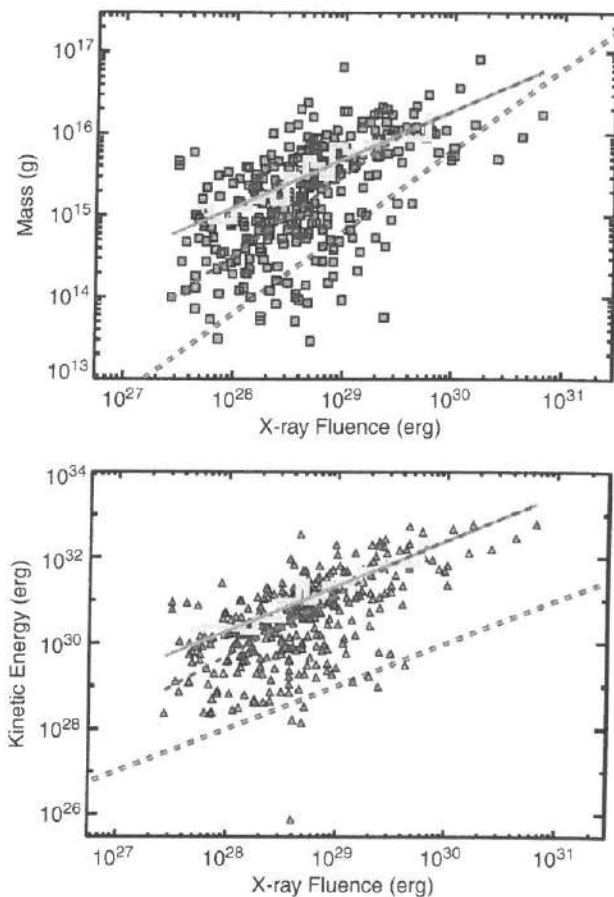


Fig. 4.10 Distribution of solar CME mass (top) and kinetic energy (bottom) as a function of flare energy. The light-gray histograms are the means over 20 data points and the solid lines are linear fits to these means. (From Drake *et al.*, 2013.)

kinetic energy fit (gray line), which suggests that the CME energy release is dominated by the mass ejection itself, and the flare energy as measured in the GOES X-ray pass band represents only a small fraction (about 1%) of the total CME energy (Schrijver *et al.*, 2012).

Solar-flare observations also reveal a power-law relation between the occurrence rate of CMEs and the associated flare energy (Drake *et al.*, 2013):

$$\frac{dn}{dE} = kE^{-\alpha}. \quad (4.5)$$

The index α is found to be between 1.5–2.5 for all stellar types and k is a normalization factor. The total flare power, P , can be obtained from the following integral:

$$P = \int E dN = \int E \frac{dN}{dE} dE = \int_{E_{min}}^{E_{max}} EkE^{-\alpha} dE = \frac{k}{2-\alpha} [E_{max}^{2-\alpha} - E_{min}^{2-\alpha}]. \quad (4.6)$$

Because for very active stars the total power in flares is assumed to dominate coronal emission, the total power P should equal the total available X-ray flux (e.g., the total X-ray luminosity, L_x), we find that the normalization constant is:

$$k = \frac{L_x(2-\alpha)}{E_{max}^{2-\alpha} - E_{min}^{2-\alpha}}. \quad (4.7)$$

Another bit of information we obtain from Yashiro and Gopalswamy (2009) is the association fraction as a function of X-ray energy, $f(E)$. This function tells us what the probability is that a CME actually erupts for a given flare energy (not every solar flare is associated with a CME: the more energetic the flare, the more likely it is there is a CME associated with it). In general, $f(E)$ can be expressed as a power-law:

$$f(E) = \zeta E^{\delta}, \quad (4.8)$$

where $\zeta = 7.9 \times 10^{-12}$, and $\delta = 0.37$ for $E \leq 3.5 \times 10^{29}$ erg, and $f(E) = 1$ for X-ray total energies higher than 3.5×10^{29} (every flare above this energy is associated with a CME). The total mass-loss rate can then be estimated by the following integral:

$$\dot{M}_{CME} = \int_{E_{min}}^{E_{max}} m_c(E) f(E) \frac{dn}{dE} dE. \quad (4.9)$$

Combining Eqs. (4.2), (4.5), (4.7), and (4.8), we obtain an expression for the stellar mass-loss rate to CMEs:

$$\dot{M}_{CME} = \mu \zeta L_x \left(\frac{2-\alpha}{1+\beta+\delta-\alpha} \right) \left[\frac{E_{max}^{1+\beta+\delta-\alpha} - E_{min}^{1+\beta+\delta-\alpha}}{E_{max}^{2-\alpha} - E_{min}^{2-\alpha}} \right]. \quad (4.10)$$

Figure 4.11 shows the range of mass-loss rates due to CMEs from Drake *et al.* (2013). It can be seen that this range is for very high mass-loss rates of $(2-4) \times 10^{-10} M_{\odot} \text{ yr}^{-1}$. Aarnio *et al.* (2012) found similar high mass-loss rates in the range of $10^{-11}-10^{-9} M_{\odot} \text{ yr}^{-1}$. These mass-loss rates are higher than the upper limit estimated for the ambient stellar wind, while the associated CME energy can reach a tenth of the total bolometric energy. Therefore, while it is possible that mass-loss processes in very active stars are dominated by CMEs, it is more likely that the solar CME-flare relation used here breaks down for higher flare energies. Drake *et al.* (2013) concluded that a more reasonable value for the associated CME energy is 1% of the total bolometric energy, which corresponds to mass-loss rate value of $5 \times 10^{-11} M_{\odot} \text{ yr}^{-1}$.

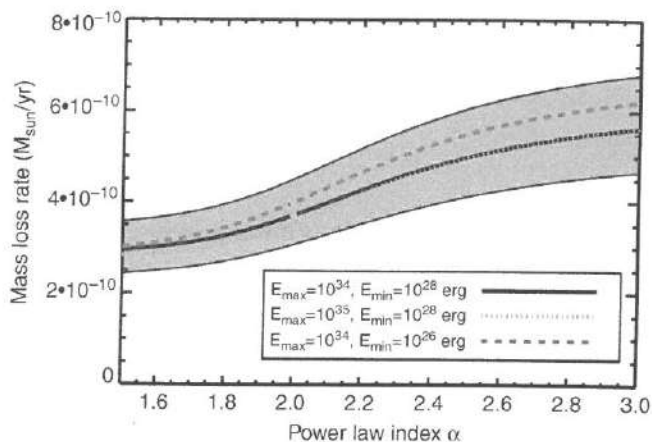


Fig. 4.11 The expected mass-loss rate due to CMEs as a function of the power index α for $L_x = 10^{30} \text{ erg s}^{-1}$ and for different maximum and minimum event energies. The gray area represents the uncertainty in the other power-law indices. (From Drake *et al.*, 2013.)

Aarnio *et al.* (2012) also estimated the torque on T-Tauri Stars (TTS) as a result of stellar mass loss to CMEs. They used the same method used to calculate the stellar spin-down rate due to the mass-loss to the ambient wind (Matt and Pudritz, 2008; Matt *et al.*, 2012), but replaced the mass-loss rate with that of CMEs. They found that the torque on the star due to CMEs, τ is:

$$\tau = k^2 \left(\frac{M_\star}{\dot{M}_{\text{CME}}} \right) \left(\frac{R_\star}{r_A} \right), \quad (4.11)$$

where M_\star is the stellar mass, R_\star is the stellar radius, r_A is the average distance to the Alfvén point, and k is a constant. They have estimated that the Alfvén radius for TTS could range between $3 R_\star$ and $70 R_\star$, and that the torque could be efficient in spinning down stars when considering an upper limit mass-loss rate due to CMEs of $\dot{M}_{\text{CME}} > 10^{-10} M_\odot \text{ yr}^{-1}$.

In the context of the Faint Young Sun paradox, it is interesting to mention a scenario at which the CME rate is very high for young, fast-rotating, active stars. If the stellar magnetic activity in such stars is concentrated at high latitudes, and the CMEs are launched at these latitudes, then we can have an efficient way to remove mass from the star without spinning the star down quickly (the torque applied on the star has a latitudinal dependence that goes to zero above and below the stellar poles). Therefore, the star can maintain its high level of activity and high CME rate, while losing a large amount of mass. This way, we may be able to demonstrate that the young Sun has been more massive in the past and solve the paradox. While the continuous mass loss cannot be high enough, transient mass-loss rate scenarios,

such as the one presented here may be sufficiently high. This is an active topic that is currently studied both theoretically and observationally using the Chandra and XMM-Newton X-ray observatories, as well as helioseismic and (*Kepler* mission) asteroseismic data.

4.3 Coronal mass ejections and close-in exoplanets

Since the mid 1990s, and through the era of the *Kepler* mission, hundreds of exoplanets have been discovered. Many of these planets are so-called “hot jupiters” – gas giant planets that orbit their parent star within a distance of less than one tenth of the Sun–Earth distance (0.1 AU). Additionally, the current search for habitable, Earth-like, rocky exoplanets is focused on planets orbiting M-dwarf stars, which are the most common in the Universe, and are very faint so their habitable zone (see Ch. 4, Vol. III) is located very close to the star, close enough that these planets can be detected by the current techniques.

Many interesting processes can arise from the close proximity of a planet to its parent star. Particularly, if the planet is magnetized, and it resides within the Alfvén point of the stellar corona. In this case, interaction between the planet and the star/stellar corona may be possible (known as star–planet interaction, SPI). Shkolnik *et al.* (2003, 2005a,b, 2008) observed an increase in coronal activity in the Ca II K line attributed to SPI in several planetary systems. There is also growing evidence that stars harboring close-in planets have excess angular momentum (Pont, 2009; Lanza, 2010), X-ray activity (Kashyap *et al.*, 2008), and EUV activity (Shkolnik, 2013). In other words, stars with close-in planets rotate faster than they should for their age, and they are also more active for their age. The excess in angular momentum can be due to tidal interaction between the star and the planet, which spins up the star, or due to a reduction in stellar magnetic braking, because the planet and its magnetosphere serve as an obstacle in the stellar corona, so the stellar spin down decreases. These findings are very important for stellar activity evolution, because they shuffle the common rotation–age–activity relation which has been used for many years. In contrast, the observational evidence for SPI is still debated. For example, Miller *et al.* (2015) performed a statistical study to test the hypothesis that planets can boost their host’s activity and found that this behavior is biased to planets that are both very massive and are extremely close to the host star, where most other cases did not show consistent increase in activity. This means that the interaction may be dominated by tidal effects and not magnetic SPI.

While all the aspects above involve very interesting plasma physics processes, in this section we focus on the unique features of the interaction between CMEs and close-in planets, and the resulting effects on both the planets and the CMEs.

4.3.1 The impact of CMEs on close-in exoplanets

Because of their close proximity to the stars, close-in planets can be eroded by CMEs and lose a significant fraction of their atmospheres (it is possible that CMEs have played a role in the loss of the Martian atmosphere; see Ch. 7 in this volume). In order to sustain an atmosphere, a planet should have a strong internal force to resist the stripping force of the CME, i.e., a strong internal magnetic field. Alternatively, it needs a thick atmosphere so that it can survive longer. While the interaction between CMEs and planets in the solar system has been studied extensively and in detail, it is not clear how CMEs impact close-in planets due to two factors. First, it is not clear how CME properties and frequencies scale with stellar properties. Second, it is hard to predict whether close-in planets would have a strong or weak internal magnetic field; there are conflicting arguments for and against each of the options (see some discussion on planetary dynamos in Ch. 6 in this volume).

Khodachenko *et al.* (2007) and Lammer *et al.* (2007) have estimated the planetary magnetic field necessary to protect the atmospheres of planets located at distances of less than 0.2 AU from erosion by CMEs. The CME density was scaled to close-in orbits based on statistical characterization of solar CMEs with possible minimum and maximum extremes as follows:

$$n_{eject}^{min} = n_0^{min} \left(\frac{d}{d_0} \right)^{-2.3}, \quad (4.12)$$

$$n_{eject}^{max} = n_0^{max} \left(\frac{d}{d_0} \right)^{-3.0}, \quad (4.13)$$

with $n_0^{min} = 4.88 \text{ cm}^{-3}$, and $n_0^{max} = 7.0 \text{ cm}^{-3}$. Here d is the orbital distance and d_0 and n_0 are the distance and density of the CME at the point of eruption. They then calculated the magnetosphere standoff distance, R_{mp} , described by the balance between the planetary magnetic pressure and the ram pressure of the CME (cf., Ch. 10 in Vol. I), $P_{CME} = n_{CME} m v_{CME}^2$. Here n_{CME} ranges between n_{eject}^{min} and n_{eject}^{max} , m is the average mass of the CME particles (taken here to be the proton mass), and $v_{CME} = 500 \text{ km s}^{-1}$ is the CME speed. The expression for R_{mp} is then (Vol. I, Eq. (10.1)):

$$R_{mp} = \left(\frac{\mu_0 f_0^2 M^2}{8\pi^2 P_{CME}} \right)^{1/6}, \quad (4.14)$$

with μ_0 being the magnetic permeability, $f_0 = 1.16$ is a numerical factor that accounts for the non-spherical shape of the magnetosphere, and M is the planetary magnetic moment. Based on these scaling laws, and estimations of the strength of the planetary magnetic moment for a given stellar mass and orbital separation, Khodachenko *et al.* (2007) have estimated the range at which the planetary magnetopause is far enough to protect the planetary atmosphere from erosion by

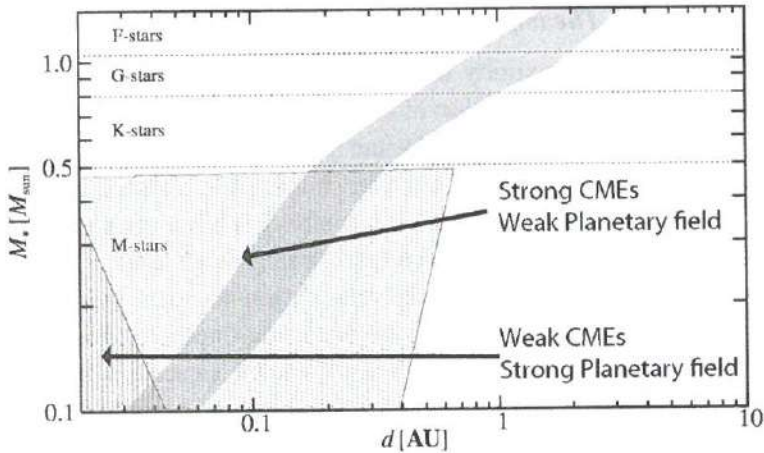


Fig. 4.12 Comparison between the habitable zone (HZ; shaded area) and the areas where strong magnetospheric compression is possible by CMEs (lightly and heavily dotted areas). The lightly dotted area indicates Earth-like exoplanets with a minimum value of the magnetic moment exposed to strong (dense) CMEs. This area denotes the region where CMEs compress the magnetosphere down to 1.15 Earth radii or less (i.e., 1000 km above the planetary surface). The heavily dotted area indicates Earth-like exoplanets with a maximum value of the magnetic moment exposed to weak (sparse) CMEs. In this region, CMEs compress the magnetosphere to less than 2 Earth radii. (From Khodachenko *et al.*, 2007.)

CMEs. Figure 4.12 shows a plot for stellar masses as a function of the orbital distance. It shows the habitable zone as shaded area, and it also shows that CMEs can erode the planetary atmosphere across a significant fraction of this area. Overall, both Khodachenko *et al.* (2007) and Lammer *et al.* (2007) concluded that planets located at an orbital distance of 0.2 AU or less would lose a significant fraction of their atmosphere unless they have a significant internal magnetic field.

Cohen *et al.* (2011) performed a numerical simulation of a CME event hitting a close-in exoplanet in order to study atmospheric protection by the planetary magnetic field for a range of field strengths. They used an MHD model that is used to simulate solar space weather events and simulated the extra-solar CME in the same manner that CMEs on the Sun are obtained. The parameters for the CME were selected based on the parameters of the May 2005 real solar CME event (a typical solar CME), where the planet was embedded in the simulation domain. Figure 4.13 shows the calculated penetration of the CME estimated by the mass flux through three spheres around the planet at distances of 0.5, 1, and 2 planetary radii above the surface. A negative value of the mass flux means that the CME has penetrated the sphere while positive flux means that the CME has not reached that height (this is a planetary outflow flux). It can be seen that for a field strength of 0.5 G (slightly larger than the Earth's magnetic field), the CME strongly penetrates at 2 planetary radii, but at 1 planetary radii or below, there is no penetration. For

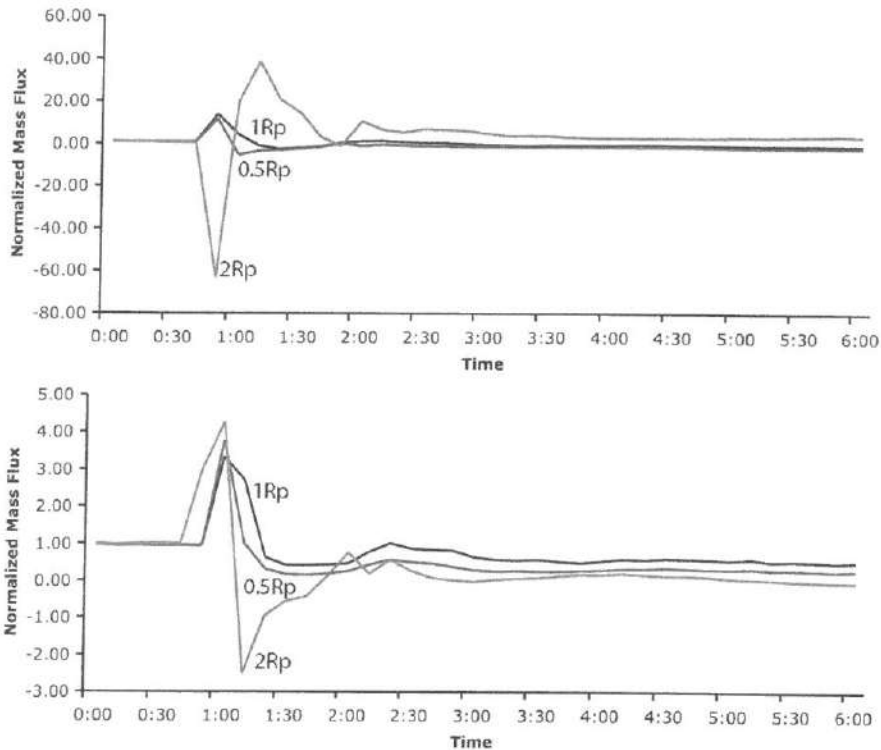


Fig. 4.13 Mass flux for a CME simulation integrated over three spheres around the impacted planet at heights of 0.5, 1, and 2 planetary radii above the surface, shown as a function of time. Fluxes are normalized to the value of the initial state at $t = 0$ (which is positive). The top panel shows results for planetary field strength of 0.5 G, and the bottom panel shows results for planetary field strength of 1 G. (From Cohen *et al.*, 2011.)

a stronger planetary field strength of 1 G, the CME barely penetrates even to 2 planetary radii above the surface.

Another interesting aspect that was noted by Cohen *et al.* (2011) is the change of magnetospheric orientation during the CME event, as shown in Fig. 4.14. Owing to their fast orbital motion, close-in magnetized planets may have their magnetotails stretched in the azimuthal direction (similar to a cometary tail). Therefore, the general orientation of the planetary magnetosphere is tilted by 45–90 degrees with respect to the radially flowing stellar wind. However, once the CME hits the planet, the magnetosphere is rotating to be radially aligned with the direction of the CME propagation trajectory. This rotation of the whole magnetosphere within a time period of less than an hour can have implications of induced currents and deposition of energy to the planetary upper atmosphere. Based on the numerical simulation, Cohen *et al.* (2011) estimated that the energy deposited onto the planet in such an event is about a thousand times higher than the energy deposited to the Earth in a typical CME event. Therefore, the interaction of CMEs with close-in planets

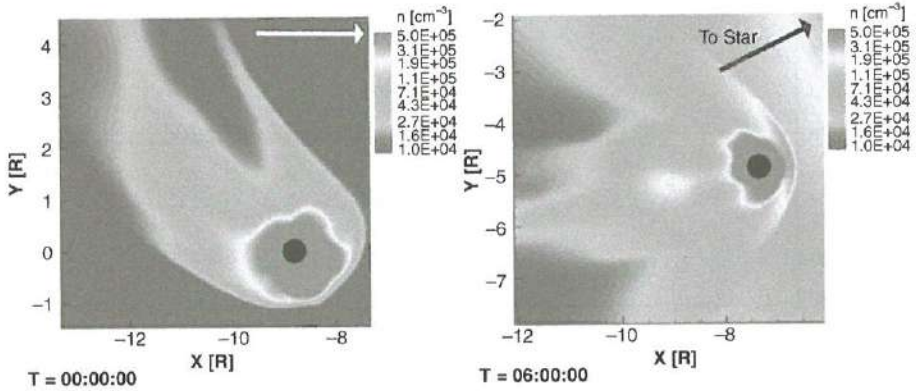


Fig. 4.14 Renderings of the number density around a close-in exoplanet shown on the equatorial plane for the initial, pre-eruption state (left), and during the CME event, 6 h after the eruption. The plot is in the Astrocentric coordinate system at which the star is located at the origin of the coordinate system. (From Cohen *et al.*, 2011.)

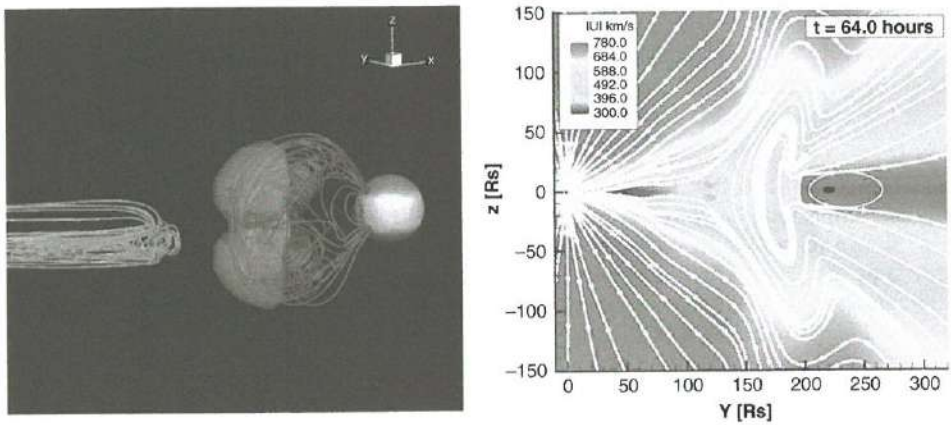


Fig. 4.15 Left: a CME approaching a planet. The star is shown on the right with selected CME field lines. The shaded volume represents an iso-surface for speed of 1500 km s^{-1} . The planet is shown as a small sphere with magnetospheric field lines shown as well. Right: meridional cut shows contours of speed between the Sun and the Earth with a small black ellipse representing the Earth's magnetosphere. (Left-hand image from Cohen *et al.*, 2011; right-hand image from Manchester *et al.*, 2004.)

could be very violent, where a significant amount of the planetary magnetosphere is stripped by the CME.

4.3.2 The effect of close-in planets on CME evolution

Another unique feature of CME–planet interaction in close-in planets is the impact on the CMEs themselves. Let us look at Fig. 4.15. On the left, we see the CME

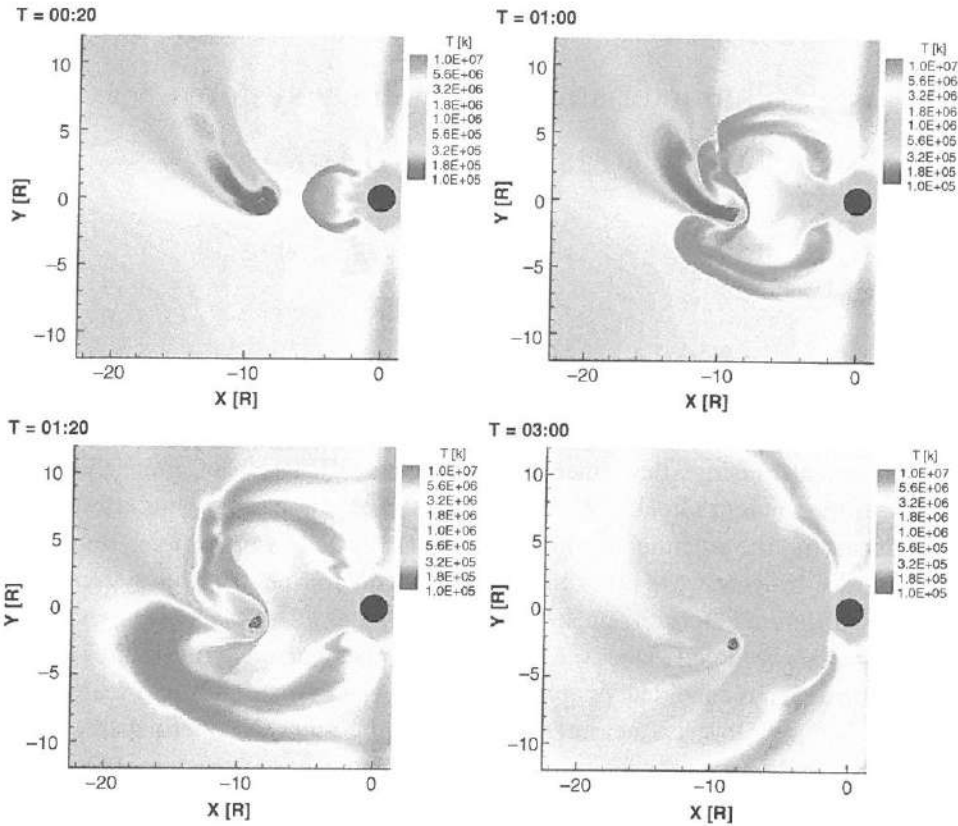


Fig. 4.16 Contours of the temperature displayed on the equatorial plane during a CME event at a close-in planet for four phases of the interaction. Coordinates are shown in units of stellar radius. (From Cohen *et al.*, 2011.)

approaching the magnetosphere of the close-in planet based on the simulation by Cohen *et al.* (2011). On the right, we see a meridional cut in the space between the Sun and the Earth taken from a simulation by Manchester *et al.* (2004). The plot shows a CME that was launched from the Sun approaching the Earth, where the small black ellipse represents the Earth's magnetosphere. Figure 4.15 demonstrates the difference in scales between the CME and the magnetosphere. By the time a CME reaches 1 AU, it is so much bigger than the Earth's magnetosphere that the interaction between them affects only the Earth. However, on close-in planets, the CME and the magnetosphere are comparable in size. As a result, the CME itself is affected by the interaction and it breaks in the middle as shown in Fig. 4.16. Because close-in planets orbit their host stars in periods of only a few days, the chance of a CME to hit a planet is rather high. If this is the case, it is possible that the interaction of CMEs and the close-in planets accelerates the dissipation of the CME as it moves into the outer astrosphere.

5

Characteristics of planetary systems

DEBRA FISCHER AND JI WANG

Philosophical musings that other worlds might exist date back more than 2000 years to the ancient Greeks. We live in a fortunate time, when the discovery of exoplanets has the potential to address questions about how planetary systems form and evolve. In what ways do exoplanetary systems mirror our solar system? How are they different? Does the presence of a binary star affect planet formation? Are Earth analogs common? Does the energy from other stars give rise to life?

Confirmed and candidate exoplanets number in the thousands and search techniques include Doppler measurements, transit photometry, microlensing, direct imaging, and astrometry. Each detection technique has some type of observational incompleteness that imposes a biased view of the underlying population of exoplanets. In some cases, statistical corrections can be applied. For example, transiting planets can only be observed if the orbital inclination is smaller than a few degrees from an edge-on configuration. However, with the reasonable assumption of randomly oriented orbits, a geometrical correction can be applied to determine the occurrence rate for all orbital inclinations. In other cases, there is simply no information about the underlying population and it is not possible to apply a meaningful correction. For example, the number of planets with a similar mass (or radius) and a similar intensity of intercepted stellar flux as our Earth is not secure at this time because the number of confirmed detections for this type of planet is vanishingly small.

As a result of the sample biases and observational incompleteness for each discovery technique, our view of exoplanet architectures is fuzzy at best. There are no cases beyond the solar system where the entire parameter space for orbiting planets has been observed. Instead, we piece together an understanding of exoplanet architectures by counting planets in the regimes where techniques are robust and then we estimate correction factors when possible. When drawing conclusions about the statistics of exoplanets, it is helpful to understand completeness in this underlying patchwork of orbital parameter space.